JOURNAL OF COMPUTATIONAL PHYSICS 98, 332–341 (1992)

Numerical Analysis of 2D MHD Equilibrium with Non-inductive Plasma Current in Tokamaks

K. TANI AND M. AZUMI

Japan Atomic Energy Research Institute, Naka-machi, Naka-gun, Ibaraki-ken, Japan 311-01

AND

R. S. DEVOTO

Lawrence Livermore National Laboratory, P.O. Box 5511, Livermore, California 94550

Received September 22, 1989; revised October 17, 1990

We have developed a numerical code to investigate steady state neutral-beam-driven, ohmic and bootstrap currents which are consistent with MHD equilibrium. The code can describe the effects of mirror trapping, energy diffusion, and bounce motion of fast ions on the beam-driven current. The bootstrap current is evaluated for multi-species ions including impurity and unthermalized fast ions. An iterative algorithm is employed to obtain a self-consistent current and MHD equilibrium. MHD stability for the converged solution can also be investigated with the code. © 1992 Academic Press, Inc.

1. INTRODUCTION

One of the most important problems for the design of steady-state tokamak reactors is the need for methods to drive plasma current non-inductively. Recent observations of substantial plasma-current driven by neutral beam injection [1, 2, 3] and lower hybrid waves [4, 5] suggest the possible development of steady-state tokamak reactors. The experimental detection of considerable neoclassical current in TFTR and JET [3, 6] can also reduce the additional power requirements for the current drive. These experimental results motivate us to analyse 2D MHD equilibrium with these non-inductive plasma currents. These currents and the MHD equilibrium, however, strongly depend on each other. Therefore, for an accurate treatment, a self-consistent analysis of 2D MHD equilibrium and the current distribution is necessary.

By applying current-drive techniques with NBI or RF waves, we can control not only the total plasma current but also the current profile. Besides the self-consistent MHD equilibrium, the dependence of MHD stability on the current profile is of great importance. Accordingly, we have developed a code, ACCOME (analyzer for current drive consistent with MHD equilibrium), version I. ACCOME employs an iterative method to deduce non-inductive currents which are consistent with MHD equilibrium. At the final step of the computation, the MHD stability for a resultant current profile is investigated analytically.

In the present paper, some details of the current drive by neutral beam injection and bootstrap effects are described in Section 2. Brief explanations of the MHD equilibrium and stability codes used in ACCOME are presented in Section 3. The iterative algorithm of ACCOME is explained in Section 4. Results of typical application of ACCOME to JT-6OU are shown in Section 5, and the conclusions of the present work are summarized in the last section of this paper.

2. PLASMA CURRENT ANALYSIS

2.1. *Beam-Driven Current*

The current density driven by neutral beam injection can be simply given by

$$\langle j_{||}^{\mathrm{BD}} \rangle = \langle j^f \rangle \, \Gamma(\psi), \tag{1}$$

where j^f is the fast-ion current density, ψ the poloidal flux function divided by 2π, and the angular brackets denote flux surface averages. The ratio of the beam-driven current to the fast-ion current Γ is approximately given by [7]

$$\Gamma \simeq 1 - \frac{Z_f}{Z_{\mathrm{eff}}}(1 - g_t), \tag{2}$$

where g_t is the trapped electron correction ($\simeq 1.4\sqrt{\varepsilon}$), Z_f is the charge number of fast ions, Z_{eff} is the effective charge number, and ε is the inverse aspect ratio. For calculation

0021-9991/92 $3.00

of the MHD equilibrium, we need the current density averaged over each flux surface, that is,

$$\frac{\langle j_{\|}^{\mathrm{BD}} B\rangle}{B_t} = \frac{\langle j^f B\rangle}{B_t} \Gamma, \tag{3}$$

where B and B_t are the local and reference toroidal magnetic fields. The current density $\langle j^f B\rangle / B_t$ in Eq. (3) can be found from

$$\frac{\langle j^f B\rangle}{B_t} = eZ_f \int_0^\infty \int_{-1}^{+1} f(v, \zeta_0, \psi) \times H(v, \zeta_0, \psi)\, v^3\, d\zeta_0\, dv, \tag{4}$$

where $f(v, \zeta_0, \psi)$ is the distribution function of fast ions in steady state, $\zeta_0 = v_{\|0}/v$, and $v_{\|0}$ is the velocity of fast ions parallel to the magnetic field line measured in the midplane. The function $H(v, \zeta_0, \psi)$ in Eq. (4) is defined as

$$H(v, \zeta_0, \psi) = \frac{1}{v} \oint \frac{B}{B_t}\, dl \Big/ \oint \frac{dl}{v_{\|}}, \tag{5}$$

where $\oint dl$ denotes the integration over a bounce motion of fast ions.

We have used two methods to solve for the distribution function of the fast ions: a method employing an orbit-following Monte-Carlo (OFMC) technique and one which uses analytic eigenfunctions of the Fokker–Planck equation. The former can precisely describe the beam-driven current, taking into account the effect of loss orbits and the charge-exchange process of fast ions while slowing down. This method, however, requires very long CPU time. For example, it takes about 2 h to analyze the beam-driven current for 2000 test particles with beam energy of the order 1 MeV on a FACOM M780 computer (speed $\simeq$ 10 MFLOPS [Linpack]). As is described in the last section, in order to obtain an MHD equilibrium which is consistent with the beam-driven current, there is no alternative but to choose an iterative method. Usually about 5–10 iterations are necessary to reach a self-consistent current and MHD equilibrium. Therefore, it is almost impossible to employ an OFMC method for this kind of calculation. On the other hand, the method which uses analytic eigenfunctions of the Fokker–Planck equation requires a very short CPU time, (about 10–20 s) with the same computer. The conventional analytical treatments [7, 8], however, have some problems in the description of fast-ion current. Results from an OFMC code [9] have indicated that the effect of particle trapping on beam-driven current is of great importance, especially for fast ions with initial pitch $(v_{\|0}/v)$ near ζ_0^t, where ζ_0^t is the pitch of the barley-trapped particles. The OFMC code shows that the current driven by fast ions with initial pitch less than ζ_0^t is almost zero. On the other hand, the conventional treatment gives a large amount of erroneous current with the same pitch. The effect of energy diffusion also becomes important as the ratio of beam energy to plasma temperature is reduced. Neither of these effects are taken into consideration in the conventional analytical codes. Accordingly, we have developed an improved semi-analytical code to derive the distribution function in Eq. (4) [9]. In general, variables of f can be separated as

$$f(v, \zeta_0, \psi) = s(\psi)\, \tau_s(\psi) \sum_n a_n(v, \psi)\, c_n(\zeta_0, \psi), \tag{6}$$

where s is the volume source of fast ions and τ_s is the slowing down time. In the velocity region $v < v_B$, $a_n(v, \psi)$ in Eq. (6) is simply given by

$$a_n(v, \psi) = \frac{1}{v^3 + v_c^3} \left[\frac{v^3}{v_B^3} \frac{v_B^3 + v_c^3}{v^3 + v_B^3} \right]^{[Z]\,\lambda n/3}, \tag{7}$$

where $v_B = \sqrt{2E_B/m_f}$, E_B is the injected beam energy, m_f the mass of beam ions, and $v_c(\psi)$ the local critical velocity;

$$[Z] = \frac{Z_{\mathrm{eff}}}{2\bar{Z}},$$

$$\bar{Z} = \frac{m_f}{\ln \Lambda_e n_e} \sum_\beta \frac{Z_\beta^2 \ln \Lambda_\beta}{m_\beta},$$

β denotes the type of ion species of bulk plasma, $\ln \Lambda_\beta$ the Coulomb logarithm for particles "β" and λ_n the nth eigenvalue described later.

In the velocity region $v > v_B$, the energy diffusion term derived by Gaffey [10] is employed; that is,

$$a_n(v) = \frac{1}{v_B^3 + v_c^3} \exp\left[- \frac{2(1 + v_c^3/v_B^3)}{T_e/E_B + (T_i/E_B)(v_c^3/v_B^3)} \frac{v - v_B}{v_B} \right]. \tag{8}$$

The bounce-averaged differential equation for c_n in Eq. (6) can be written as [11]

$$\frac{1}{R(\zeta_0, \zeta_0^t)} \frac{d}{d\zeta_0} \left[(1 - \zeta_0^2)\, Q(\zeta_0, \zeta_0^t) \frac{dc_n}{d\zeta_0} \right] + \lambda_n c_n = 0, \tag{9}$$

where

$$R(\zeta_0, \zeta_0^t) = \frac{2}{\pi} K\left[\left(\frac{\zeta_0^t}{\zeta_0} \right)^2 \right],$$

$$Q(\zeta_0, \zeta_0^t) = \frac{2}{\pi} E\left[\left(\frac{\zeta_0^t}{\zeta_0} \right)^2 \right],$$

K and E are the complete elliptic integral of the first and the

second kind, respectively. The effect of bounce motion of fast ions as well as the effect of particle trapping are taken into consideration in Eq. (9). We derive these eigenfunctions $c_n(\psi)$ and eigenvalues λ_n numerically by adopting a variational method [9].

Another important calculation for obtaining beam-driven current is the fast-ion source term $s(\psi)$ in Eq. (6). ACCOME can treat parallel and elliptical cross-sectional neutral beams with horizontal and vertical radii a_B and b_B. Here we introduce polar coordinates θ_B and

$$r_B = \sqrt{x^2 + y^2 a_B^2 / b_B^2},$$

where (x, y) are the horizontal and vertical coordinates in the beam cross section. The local fast-ion source term can be derived by calculating the total fraction of neutral beams trapped in a plasma S. The latter is given by

$$S = \sum_j \sum_k \gamma_{kj} \int_0^{L_{\max}} \int_0^{2\pi} \int_0^{a_B} w(r_B, \theta_B) \times \exp\left[-\int_0^{L_B} n_e(\psi)\, \sigma_s\, dL \right] \times n_e(\psi)\, \sigma_s r_B\, dr_B\, d\theta_B\, dL_B, \tag{10}$$

where L_B is the beam path length, $L_{\max}$ is the maximum beam path length which intersects the plasma column, a_B is the neutral beam radius, γ_{kj} is the density fraction of the jth neutral beam with energy of E_B/k, E_B is the primary beam energy, σ_s is the stopping cross section, and $w(r_B, \theta_B)$ is the normalized distribution of beam density defined by

$$\int_0^{a_B} \int_0^{2\pi} w(r_B, \theta_B)\, r_B\, dr_B\, d\theta_B = 1.0.$$

The stopping cross section σ_s is given by the numerical fit by Janev *et al.* [12]. Here we consider a neutral beam with beam-density distribution of the form

$$w(r_B, \theta_B) = \frac{1.582}{\pi a_B^2} \exp[1 - (r_B/a_B)^2]. \tag{11}$$

Introducing new variables

$$r'_B = \sqrt{1.582[1 - \exp(-(r_B/a_B)^2)]}$$
$$\theta'_B = \theta_B / 2\pi$$
$$L'_B = L_B / L_{\max}$$

and, substituting Eq. (11) into Eq. (10), we obtain

$$S = 2L_{\max} \sum_j \sum_k \gamma_{kj} \int_0^1 \int_0^1 \int_0^1 \exp\left[-L_{\max} \int_0^{L_B} n_e(\psi)\, \sigma_s\, dL \right] \times n_e(\psi)\, \sigma_s r'_B\, dr'_B\, d\theta'_B\, dL'_B. \tag{12}$$

These integrals are evaluated with a Monte-Carlo integration method. Six uniform random numbers corresponding to r_B, θ_B, L_B, beam number, beam ion species k, and co-injection fraction are generated for every sampling point. The calculation of Eq. (4) is executed for every test particle. Consequently, the total number of test particles is limited within about 2000, due to the long computational time for the current drive.

The beam-driven current derived from the new semi-analytical treatment is compared with that from the OFMC code [9]. Both results agree very well if the effect of the charge-exchange loss of fast ions is not taken into consideration. The difference between the total currents with and without the charge-exchange process is only 3–4% in a reactor-grade tokamak.

2.2. *Bootstrap Current*

In ACCOME, we numerically evaluate the bootstrap current for multi-species ions, including fast ions, on the basis of the Hirshman–Sigmar moment approach of the neoclassical theory [13].

The particle and heat flow equations parallel to the magnetic field are expressed by the coupled matrix equations,

$$\sum_\beta \begin{pmatrix} l_{11}^{\alpha\beta} & l_{12}^{\alpha\beta} \\ l_{21}^{\alpha\beta} & l_{22}^{\alpha\beta} \end{pmatrix} \begin{pmatrix} \langle B \cdot u_{\|\beta} \rangle \\ -2/5 p_\beta \cdot \langle B \cdot q_{\|\beta} \rangle \end{pmatrix} = \begin{pmatrix} \mu_{11}^{\alpha} & \mu_{12}^{\alpha} \\ \mu_{21}^{\alpha} & \mu_{22}^{\alpha} \end{pmatrix} \begin{pmatrix} \langle B \cdot u_{\|\alpha} \rangle + B \cdot V_{1\alpha} \\ -2/5 p_\alpha \cdot \langle B \cdot q_{\|\alpha} \rangle + B \cdot V_{2\alpha} \end{pmatrix}, \tag{13}$$

where $u_{\|\alpha}$, $q_{\|\alpha}$, and p_α are the parallel flow velocity, the parallel heat flow, and pressure of the particle of specie "α," respectively. The coefficient $l_{ij}^{\alpha\beta}$ describes the friction between particles "α" and "β" and μ_{ij}^{α} describes the viscosity coefficient for the particle type "α," respectively. The angular bracket denotes the quantity averaged over a magnetic surface. $V_{1\alpha}$ and $-5p_\alpha/2 \cdot V_{2\alpha}$ are poloidal components of perpendicular particle flow $u_{\perp\alpha}$ and heat flow $q_{\perp\alpha}$. For particles with Maxwellian velocity distribution, friction and viscosity coefficients are explicitly derived by Hirshman and Sigmar [13]. We employ an energy-partitioning integral formula for viscosity coefficients in the banana-plateau regime with numerical factor of 2.48 proposed by Kim *et al.* [14], which gives a good agreement with the Hinton–Hazeltine formulation [15], in the limit of the large aspect ratio with $Z_{\text{eff}} = 1$. For simplicity in the calculation, we employ an analytical fitting function for the trapped particle fraction f_t [16].

In addition to Maxwellian particles, we include the effect of fast ions with an isotropic velocity distribution of the form

$$f_{f0} = \frac{n_f \tau_s}{4\pi \tau_{\text{th}} (v^3 + v_c^3)} \qquad (0 < v \leqslant v_B),$$

where n_f is the fast ion density and τ_{th} is the thermalization time. The first-order distribution function with respect to the Larmor radius can be expressed by

$$\tilde{f}_f(\upsilon, \zeta, \psi) = -\frac{R_t B_t \upsilon_{||}}{\Omega_f}\frac{\partial f_{f0}}{\partial \psi} \pm \frac{\upsilon}{2}\sqrt{\langle B^2\rangle}\, G(\upsilon, \psi) f_{f0}(\upsilon, \psi)\int_{\chi}^{\chi_c}\frac{d\chi}{\langle|\zeta|\rangle},$$

where

$$\zeta = \frac{\upsilon_{||}}{\upsilon} = \pm\sqrt{1-\chi B},$$

$$\chi = \frac{\mu_m}{E},$$

μ_m, E, and Ω_f are the magnetic moment, the energy, and the Larmor frequency of fast ions, respectively. The velocity dependence of G is determined from the velocity moments of fast ions. The effective temperature profile of fast ions is much broader than their pressure profile in a usual situation and the fast-ion induced bootstrap current is considered to be mainly driven by pressure gradient. Therefore, in the present paper, we take into account only the parallel flow balance of fast ions and neglect the parallel heat flow balance. In this approximation, G is given by

$$G = \frac{1}{f_c\sqrt{\langle B^2\rangle}}\frac{n_f m_f}{p_f}[\langle B\cdot u_{||f}\rangle - B\cdot V_{1f}],$$

where

$$V_{1f} = -\frac{R_t B_t}{\Omega_f}\frac{1}{n_f m_f}\left[\frac{\partial p_f}{\partial\psi} + e_f n_f \frac{\partial\phi}{\partial\psi}\right]$$

and $f_c = 1 - f_t$. By using the approximation of $\upsilon_i \ll \upsilon \ll \upsilon_e$, the parallel momentum balance equation of fast ions is

$$\sum_{\alpha = e,i} l_{11}^{f\alpha}(\langle B\cdot u_{||\alpha}\rangle - \langle B\cdot u_{||f}\rangle) = \mu_{11}^{f}(\langle B\cdot u_{||f}\rangle + B\cdot V_{1f}), \tag{14}$$

where friction and viscosity coefficients of the fast ion are expressed as

$$l_{11}^{fe} = l_{11}^{ef} = \frac{n_e m_e}{\tau_{ee}}\frac{Z_f^2 n_f}{n_e},$$

$$l_{11}^{fi} = l_{11}^{if} = \frac{3\sqrt{\pi}}{4}\frac{n_i m_i}{\tau_{ii}}\frac{Z_f^2 n_f}{Z_i^2 n_i}\left(1+\frac{m_i}{m_f}\right)\frac{\tau_s}{3\tau_{th}}\frac{\upsilon_i^3}{\upsilon_c^3},$$

$$\mu_{11}^{f} = \frac{f_t}{f_c}\frac{n_e m_e}{\tau_{ee}}\frac{Z_f^2 n_f}{n_e}\frac{\tau_s}{3\tau_{th}}\frac{n_f m_f \hat{Z}\upsilon_c^3}{2p_f}\int_0^{\upsilon_B}\frac{\upsilon\, d\upsilon}{\upsilon^3+\upsilon_c^3},$$

$$\hat{Z} = \sum_i Z_i^2 n_i \Big/ \sum_i Z_i^2 n_i \frac{m_f}{m_i}.$$

Remaining coefficients, such as l_{12}^{fe} and μ_{12}^{f}, are set to be zero in our approximation. Above expressions are very similar to those derived by Hirshman and Sigmar for the evaluation of beam-driven current, where they used the first Legendre moment of the beam distribution function.

The coupled matrix Eq. (13), including the fast ion Eq. (14) and its counterpart terms for Maxwellian particles, are solved numerically by a matrix inversion technique and the transport coefficients for bootstrap current, L_{31}^a and L_{32}^a ($a = e, i, f$), are evaluated. Finally, the bootstrap current $\langle J_{||}^{BS}\cdot B\rangle$ is calculated as

$$\langle J_{||}^{BS}\cdot B\rangle = \sum_a e_a n_a \langle u_{||a}\cdot B\rangle = -R_t B_t p_e \sum_a \frac{T_a}{|Z_a|\, T_e}\times\left(L_{31}^a\frac{\partial}{\partial\psi}\ln p_a + L_{32}^a\frac{\partial}{\partial\psi}\ln T_a\right). \tag{15}$$

The effective temperature T_f is defined by $T_f = p_f/n_f$. We note that $L_{32}^f = 0$ because of our approximation of neglecting the temperature gradient terms for fast ions.

ACCOME has another option for the estimation of bootstrap current, that is, the banana-plateau expressions of Hinton and Hazeltine [15], in which the multi-ion plasma is replaced with a single ion of charge Z_{eff}.

2.3. *Ohmic Current*

The flux surface averaged Faraday's law in a steady state tokamak can be written as

$$\langle j_{||}^{OH} B\rangle = \frac{V_{loop}}{\eta} F R_t \langle R^{-2}\rangle, \tag{16}$$

where F is the toroidal field function, R_t is the geometric major radius, V_{loop} is the one-turn voltage, and η is the resistivity. We assume that the resistivity is only a function of ψ and that the neoclassical effect is included [16].

3. MHD EQUILIBRIUM AND STABILITY CHECK

In order to save CPU time in computing the MHD equilibrium, ACCOME uses a very fast MHD equilibrium code which is called SELENE [17]. SELENE solves the Grad–Shafranov equation in cylindrical coordinates (R, Z) by using a combination of the DCR (double cyclic reduction) method and the Green function method for prescribed values of $p' = dp/d\psi$, $\langle J\cdot B\rangle$, and marker points on the plasma surface. SELENE employs a rectangular domain in the (R, Z) space which is divided into $2^m \times 2^n$ with equal spacing, where m and n are integers (typically $m = n = 7$).

The poloidal flux function ψ is divided into the contribution from the plasma current, ψ_p, and that from the poloidal coil currents, ψ_v; that is,

$$\psi = \psi_p + \sum_k I_v^k \cdot \psi_v^k,$$

where I_v^k and ψ_v^k are the poloidal coil current and the poloidal flux function produced by unit coil current, respectively. Without the input data for poloidal coils, SELENE generates analytic solutions of ψ_v^k that are linearly independent with each other. The basic calculation procedure of SELENE is:

(1) At first, the toroidal plasma current density j_φ at each grid in the box is evaluated with a guessed value for ψ.

(2) The value of ψ_p on the boundary of calculation domain is evaluated from the line integral along the plasma surface by using the Green function method.

(3) At this moment, the total plasma currents evaluated by the surface integral of j_φ and the line integral of $|\nabla\psi/R|$ are adjusted to the prescribed value I_p by multiplying $\langle J \cdot B \rangle$ by the proper constant.

(4) Then ψ_p is solved by the DCR matrix inversion technique.

(5) Finally, the total value of ψ at each grid is obtained by adding the contributions of ψ_v^k, where coil currents I_v^k are adjusted so that the plasma surface is through the prescribed marker points, such as the innermost/outermost minor radii, separatrix point, and so on, which are defined by the input data.

These steps are repeated until ψ at each grid converges within an allowable error ε_{eq}: $\max |(\psi_{i,j}^n - \psi_{i,j}^{n-1})/\psi_{i,j}^n| < \varepsilon_{eq}$, where i and j are the grid numbers. Typically, we set $\varepsilon_{eq} = 10^{-3}$.

For the converged equilibrium, the code checks the stability of the infinite-n ideal ballooning mode and interchange mode. For reference, tearing mode stabilities are also tested by evaluating cylindrical Δ' for the obtained safety factor profile.

4. CALCULATION PROCEDURE

As is described in the last section, all the types of plasma current depend on the geometry of MHD equilibrium. On the other hand, the MHD equilibrium directly depends on those current profiles. Therefore, we employ an iterative procedure to obtain an MHD solution which is consistent with the computed plasma currents.

In ACCOME, plasma densities and temperatures are assumed to be given by fixed functional forms of a normalized effective minor radius ρ. The variable ρ is defined as $\rho = \sqrt{V(\psi)/V_{tot}}$, where $V(\psi)$ is the plasma volume within ψ and V_{tot} is the value of V at the plasma surface. Consequently, the pressure of bulk plasma p^{th} is also given by a function of ρ. In the presence of tritons and deuterons, the pressure of unthermalized alpha particles p^α is calculated by using an analytical solution of the Fokker–Planck equation and the local fusion reaction rate.

The MHD equilibrium is solved with a restriction that the total plasma current I_p is kept constant at every iteration step. ACCOME has two options to keep the total plasma current constant: one is to regulate one-turn voltage V_{loop} with given neutral-beam power input P_{NBI} and the other is to regulate P_{NBI} with fixed V_{loop}.

From the geometric properties of the desired solution, i.e., plasma elongation κ, triangularity δ, major radius R_t, minor radius a, and plasma current I_p, we set up a Solov'ev model equilibrium. With the old MHD equilibrium of the ith iteration ψ_i, the flux-surface-averaged beam-driven current $\langle j_{||}^f B \rangle_i$, $\langle j_{||}^{BD} B \rangle_i$, bootstrap current $\langle j_{||}^{BS} B \rangle_i$, and ohmic current $\langle j_{||}^{OH} B \rangle_i$ are calculated. During the calculation process for beam-driven current, the additional pressure due to unthermalized fast ions p^f and the fast-ion density n_f are also calculated. In order to keep the plasma neutral in the presence of the injected fast ions, the electron density is reset at every iteration step as

$$n_e^{th}(\rho) = n_e^{th}|_{fixed}(\rho) + 2.0 n_\alpha(\rho) + Z_f n_f(\rho).$$

Since we employ a Monte-Carlo method to evaluate the birth profile of fast ions, the solution of $\langle j_{||}^{BD} B \rangle_i$ involves Monte-Carlo noise. In order to reduce the error bar, we use an averaging technique in the iterative procedure. The beam-driven current at the ith iteration is given as

$$[\langle j_{||}^{BD} B \rangle]_i = \frac{1}{i} \langle j_{||}^{BD} B \rangle_i + \frac{i-1}{i} [\langle j_{||}^{BD} B \rangle]_{i-1},$$

where $[X]_i$ denotes

$$\frac{1}{i} \sum_j^i X_j.$$

The same technique is adapted to the bootstrap current and the total plasma pressure

$$[\langle j_{||}^{BS} B \rangle]_i = \frac{1}{i} \langle j_{||}^{BS} B \rangle_i + \frac{i-1}{i} [\langle j_{||}^{BS} B \rangle]_{i-1},$$

$$[p]_i = \frac{1}{i} p_i + \frac{i-1}{i} [p]_{i-1},$$

where $p = p^{th} + p^\alpha + p^f$. Then the total plasma current is given by

$$\langle j_{||} B \rangle_i = [\langle j_{||}^{BD} B \rangle]_i + [\langle j_{||}^{BS} B \rangle]_i + \langle j_{||}^{OH} B \rangle_i.$$

From these quantities and the old values of the toroidal field function F_i and $\langle B^2\rangle_i$, we can compute the first derivative of the plasma pressure $[p]'_i$ and the quantity

$$F_iF'_i = -\mu_0(F_i^2[p]'_i + F_i\langle j_{||}B\rangle_i)/\langle B^2\rangle_i \qquad (16)$$

and use them to solve the Grad–Shafranov equation

$$\Delta^*\psi_{i+1} = -\mu_0 R^2[p]'_i - F_iF'_i. \qquad (17)$$

All components of plasma current are calculated again with the new MHD equilibrium. These calculation of plasma current and MHD equilibrium are executed iteratively until the value of $\langle j_{||}B\rangle$ at each radial mesh point is converged well; that is,

$$|(\langle j_{||}B\rangle_i - \langle j_{||}B\rangle_{i-1})/\langle j_{||}B\rangle_i| < \varepsilon_c$$

where ε_c is usually set at $\lesssim 10^{-2}$. With the converged values of $\langle j_{||}B\rangle$, the respective toroidal current densities are given by

$$j_\varphi = \frac{1}{2\pi}\frac{F}{\langle B^2\rangle}\left\langle\frac{1}{R^2}\right\rangle\langle j_{||}B\rangle\frac{dV}{dA},$$

$$j_\varphi^{\mathrm{OH}} = \frac{1}{2\pi}\frac{F}{\langle B^2\rangle}\left\langle\frac{1}{R^2}\right\rangle\langle j_{||}^{\mathrm{OH}}B\rangle\frac{dV}{dA},$$

$$j_\varphi^{\mathrm{BD}} = \frac{1}{2\pi}\frac{F}{\langle B^2\rangle}\left\langle\frac{1}{R^2}\right\rangle[\langle j_{||}^{\mathrm{BD}}B\rangle]\frac{dV}{dA},$$

$$j_\varphi^{\mathrm{BS}} = \frac{1}{2\pi}\frac{F}{\langle B^2\rangle}\left\langle\frac{1}{R^2}\right\rangle[\langle j_{||}^{\mathrm{BS}}B\rangle]\frac{dV}{dA},$$

where A is the area of poloidal cross section within ψ. Finally, MHD stability for the converged current profile are investigated with the method described in the last subsection. The above mentioned calculation procedure is summarized in Fig. 1.

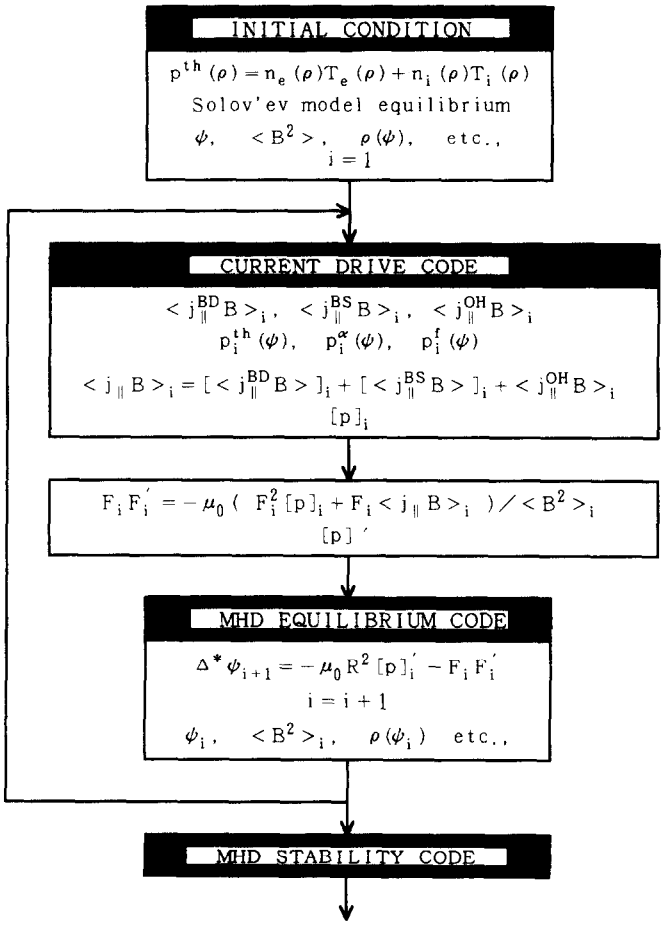

FIG. 1. Calculation procedure to obtain non-inductively driven currents which are consistent with MHD equilibrium.

5. APPLICATION RESULTS

Applications of ACCOME have been made for calculation parameters appropriate to JT-6OU which are summarized in Table I. The geometry of neutral beam line is shown in Fig. 2. Neutral deuteron beams are injected tangentially with tangency radius $R_{\tan} = 2.7$ m and energy $E_B = 400$ keV without notice. The center line of the beam is contained in the midplane. In all the subsections except Section 5.2, we choose the option of NBI power regulation to keep the total plasma current constant without ohmic current ($V_{\mathrm{loop}} = 0.0$).

TABLE I

Calcultion Parameters

Major radius	$R_t = 3.36$ m
Minor radius	$a = 1.0$ m
Toroidal field	$B_t = 4.3$ T
Plasma temperature	$T_e(\rho) = T_{e0}(1-\rho^2)$ $T_i(\rho) = T_{i0}(1-\rho^2)$ $T_{e0} = T_{i0} = 10$ keV
Plasma density	$n_e(\rho) = n_{e0}(1-\rho^2)^{0.5}$ $n_{e0} = 10^{18} - 1.5\times10^{20}$ m^{-3}
Plasma current	$I_p(I_{\mathrm{tot}}) = 2.4 - 3.6$ MA
Ellipticity	$\kappa = 1.54$
Triangularity	$\Delta = 0.35$
Bulk ions	Deuterons
Effective Z	$Z_{\mathrm{eff}} = 2.0$ (uniform)
Charge number of impurity ion	$Z_{\mathrm{imp}} = 8.0$ (oxygen)

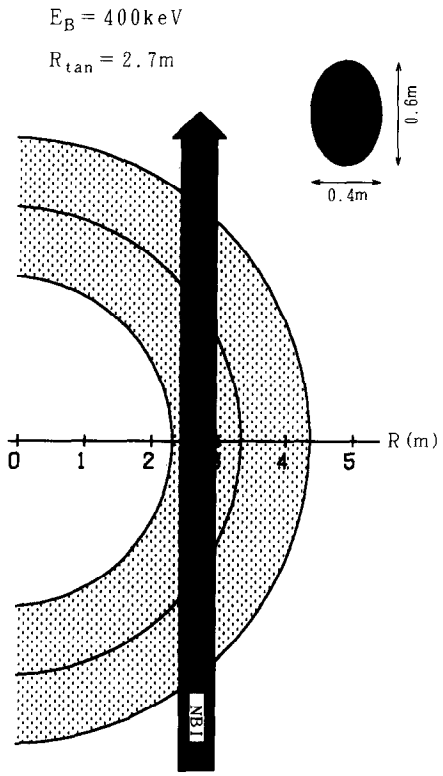

FIG. 2. Geometry of neutral beam line in JT-60U.

5.1. *Check for the Iterative Algorithm*

In advance of the application, we have tested the convergence characteristic of the iterative algorithm of ACCOME. The poloidal-beta β_p value, which is a good measure of the plasma–current profile, is plotted against the iteration number N_{it} in Fig. 3. The ratio of the neoclassical current to the total I_{BS}/I_{tot} is also plotted. The convergence

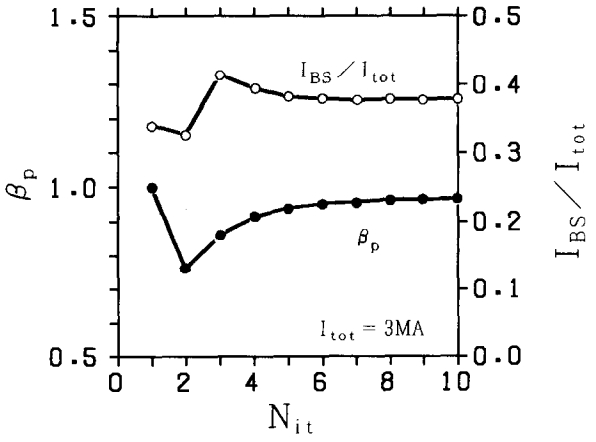

FIG. 3. Poloidal beta and ratio of bootstrap current to the total against iteration number.

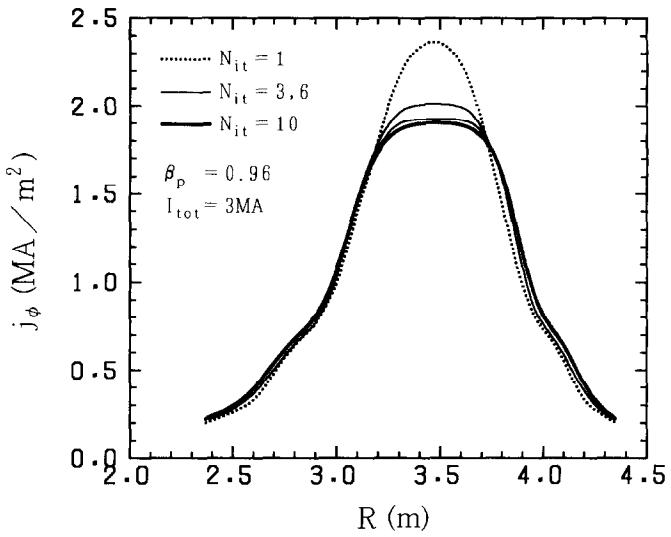

FIG. 4. Convergence process of toroidal current density for iteration step $N_{it} = 1, 3, 6$, and 10.

properties of the toroidal current density j_φ is shown in Fig. 4 for various iteration steps. It follows from those results shown in Figs. 3 and 4 that more than five iterations are necessary to obtain a plasma current profile which is consistent with MHD equilibrium.

5.2. *Effect of Particle Trapping and Energy Diffusion*

Effects of particle trapping (P.T.) and energy diffusion (E.D.) of fast ions on the beam driven current are investigated in the mode of one-turn voltage regulation with $P_{NBI} = 20$ MW and for the volume-averaged density $\bar{n}_e \simeq 5.5 \times 10^{19}$ m^{-3} ($n_{e0} = 8.0 \times 10^{19}$ m^{-3}).

The radial distribution of beam-driven current calculated with both effects, j_{BD}(P.T., E.D.), is shown in Fig. 5 by the solid curve. The distribution of beam-driven current without the effect of P.T., j_{BD}(—, E.D.), is also shown by the dash-dotted curve. The degradation of current density by the effect of P.T. can be evaluated by

$$[j_{BD}(—, \text{E.D.}) - j_{BD}(\text{P.T., E.D.})]/j_{BD}(\text{P.T., E.D.}).$$

The above ratio becomes very large in the outer core region because the particle-trapping region ($v_{||0}/v < \zeta_0^t$) increases with the local inverse aspect ratio. For reference, the distribution of beam-driven current obtained by an OFMC code is also shown in Fig. 5 by the dotted curve. The distribution of the beam-driven current estimated by the improved semi-analytical model including both the effects of P.T. and E.D. agrees very well with that from an OFMC code. Figure 6 shows the total beam-driven current and the regulated loop voltage to drive $I_{tot} = 3$MA against the injected beam energy E_B. The solid curves show the results with both the effects of P.T. and E.D., the dash-dotted curves

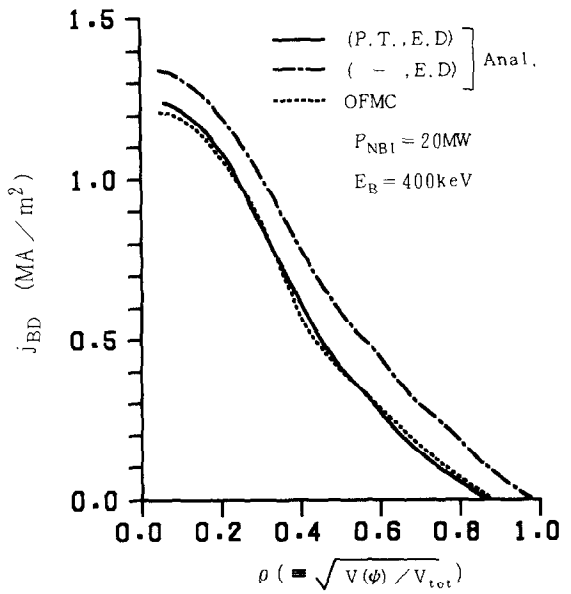

FIG. 5. Radial distribution of beam-driven current for $P_{NBI} = 20$ MW, $E_B = 400$ keV and volume-averaged density $\bar{n}_e \simeq 5.5 \times 10^{19}$ m^{-3}. Result from the improved semi-analytical code with both effects of particle trapping and energy diffusion and the one with the effect of energy diffusion only are shown by (———) and (— · —), respectively. Result from an orbit-following Monte-Carlo code is shown by (-----).

those with the effect of E.D. only, and the dashed curves those with the effect of P.T. only. The degradation of beam-driven current by particle trapping is approximately proportional to τ_{th}/τ_{fi} ($\propto \ln[1 + (E_B/E_c)^{3/2}](T_e/E_B)^{3/2}$), where τ_{fi} is the collision time between fast ions and bulk ions. Therefore, the ratio of the beam-driven current calculated without the effect of P.T. to the one with both the effects of P.T. and E.D., I_{BD}(—, E.D.)/I_{BD}(P.T., E.D.), becomes very large as E_B decreases. Figure 6 shows that the ratio can exceed 2.0 for $E_B/T_{e0} < 10$. It must be noted that the ratio is as large as 1.3 even for a higher $E_B/T_{e0} = 40$.

As is shown in Eq. (8), the contribution of energy diffusion to the beam-driven current increases with T_i/E_B and/or T_e/E_B. The ratio of the beam-driven current calculated with the effect of E.D. to the one without, I_{BD}(P.T., E.D.)/I_{BD}(P.T., —), is about 1.4 for $E_B/T_{e0,i0} \simeq 10$ and becomes less than 1.05 for $E_B/T_{e0,i0} > 30$. The effect of energy diffusion is also important for low $E_B/T_{e0,i0}$, but it is not as important as that of particle trapping.

Figure 6 also shows that, due to the large difference between beam-driven currents with and without the effect of P.T., a substantial difference between respective loop voltages to drive $I_{tot} = 3$MA is estimated. These calculation results indicate that the effect of particle trapping on the beam driven current or the one-turn voltage is of great importance for detailed analysis of the experimental data.

5.3. *Bootstrap Current*

The injected neutral beam power P_{NBI} necessary to drive full non-inductive plasma current has been investigated. In Fig. 7, the results are plotted against $\bar{n}_e$, the volume-averaged plasma density, for various I_{tot}. The solid and dotted curves are those with and without the contribution of unthermalized fast ions on the bootstrap current, respec-

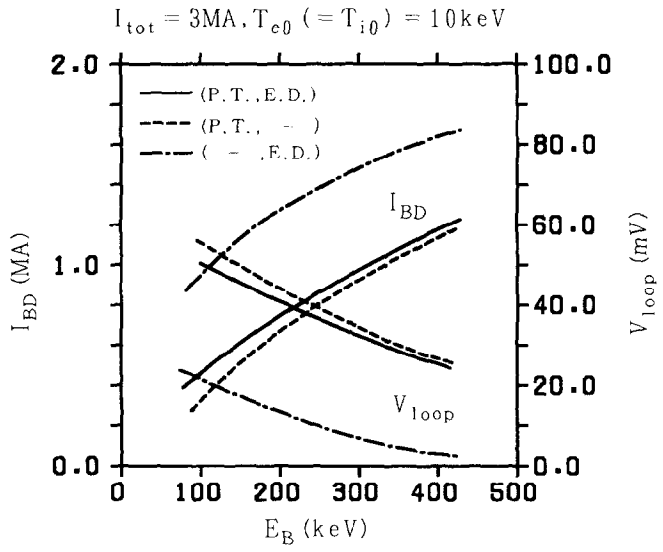

FIG. 6. Total beam-driven current and regulated loop voltage to drive $I_{tot} = 3$ MA against beam energy E_B for volume-averaged density $\bar{n}_e \simeq 5.5 \times 10^{19}$ m^{-3}. The solid curves are the results with both effects of particle trapping (P.T.) and energy diffusion (E.D.), dash-dotted curves those with the effect of E.D. only and dashed curves those with the effect of P.T. only.

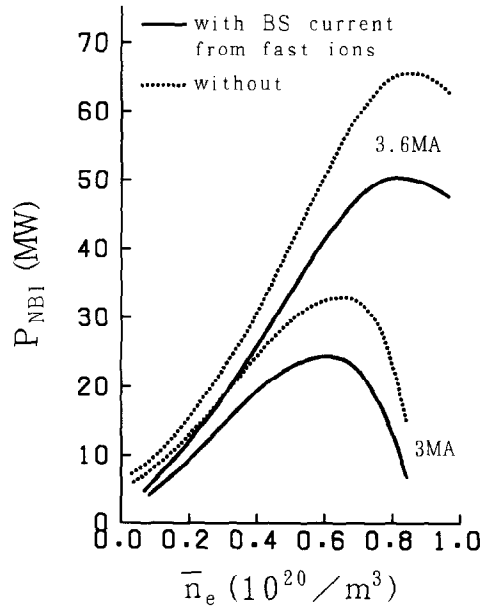

FIG. 7. Neutral beam power to drive full non-inductive plasma current I_{tot} against volume-averaged plasma density for various I_{tot}; the solid curves with the effect of unthermalized fast ions on the bootstrap current and the dotted curves without.

tively. The reduction of P_{NBI} in the high $\bar{n}_e$ region is due to the increase of bootstrap current with β_p. In the low density region, we can expect a high efficiency of beam-driven current because of the long slowing-down time. The shine-through of injected neutral beams, however, reduces the efficiency of beam deposition. These two conflicting effects cause the finite P_{NBI} at low $\bar{n}_e$.

The ratios of I_{BS}/I_{tot} with the contribution of unthermalized fast ions to the neoclassical current, are shown in Fig. 8 for $I_{tot} = 3.0$ (closed circles) and 3.6MA (open circles). In spite of the differences in I_{tot}, the ratios I_{BS}/I_{tot} for these two currents are approximately on the same curve. It must be noted that the linearity of the self-consistent I_{BS}/I_{tot} with respect to β_p is broken in both high β_p ($\beta_p > 1.4$) and low β_p ($\beta_p < 0.4$) regions. For reference, I_{BS}/I_{tot} with a fixed $j(\psi)$ profile is shown by the solid line in Fig. 8 and shows complete linearity with β_p. In general, the bootstrap current flatten the distribution of the safety factor q, especially in the high β_p region where the bootstrap current dominates the total current. The ratio $q(0)/q(0.95)$ for $I_{tot} = 3$ MA is also shown by the dashed curve in Fig. 8. Theoretical predictions [13, 15] show that the local bootstrap current is increased with the local q. This non-linear effect breaks the linear dependence of I_{BS} on β_p in the high β_p region. The β_p dependence of I_{BS}/I_{tot} shown in Fig. 8 is investigated by changing n_e. As is shown by the dotted curve, the fraction of the beta poloidal for unthermalized fast ions β_p^f becomes very large in the low β_p region. Although a substantial frac-

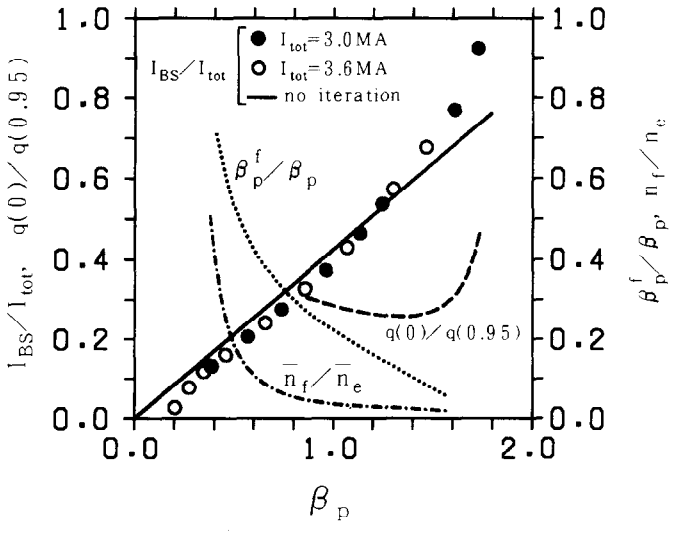

FIG. 8. Ratios of the bootstrap current I_{BS} to the total current I_{tot} against beta poloidal β_p for $I_{tot} = 3.0$ MA (●), and 3.6 MA (○). The solid line shows I_{BS}/I_{tot} for a given MHD equilibrium profile without iteration. The dashed, dotted, and dash-dotted curves show the indication of safety-factor profile $q(0)/q(0.95)$, the contribution of unthermalized beam ions to the total beta poloidal β_p^f/β_p and the ratio of the volume averaged density of fast ions to the volume averaged electron density $\bar{n}_f/\bar{n}_e$ for $I_{tot} = 3.0$ MA, respectively.

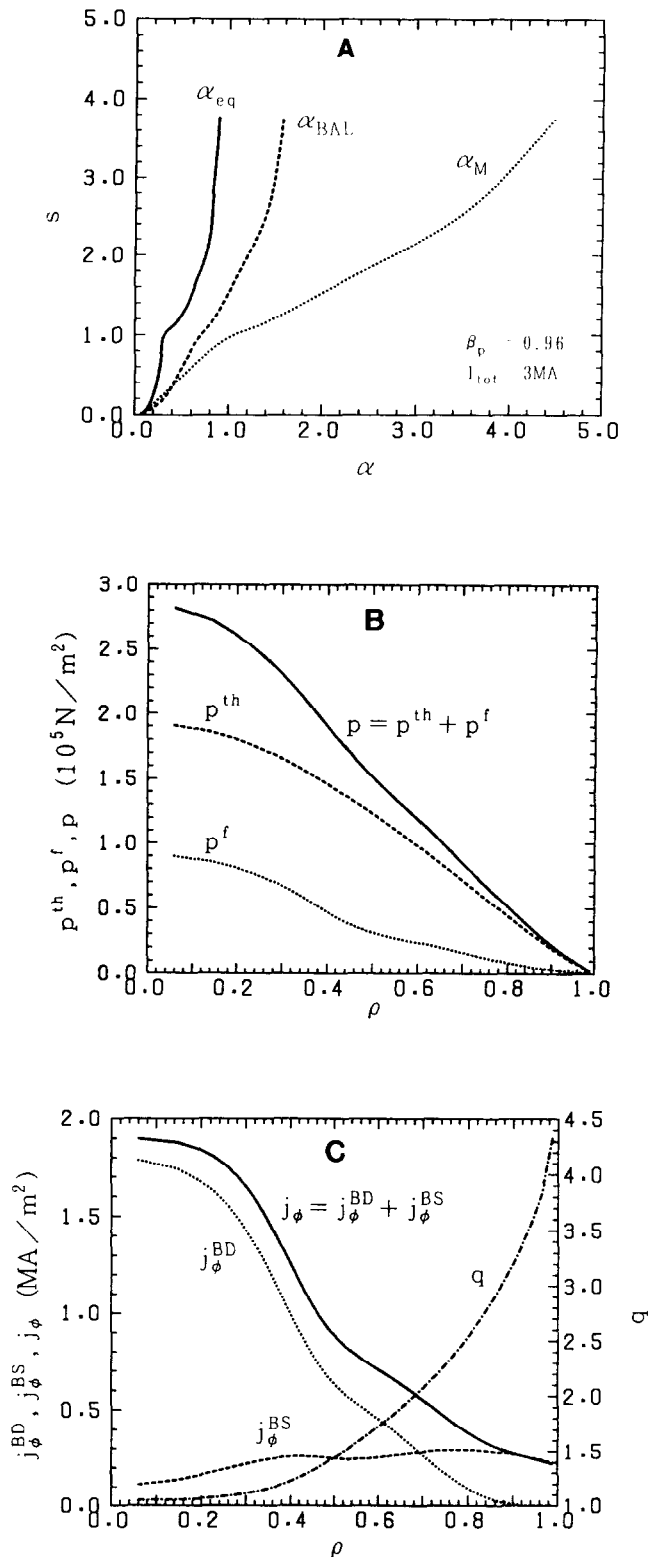

FIG. 9. Maximum stable pressure gradient for Mercier mode α_M (dotted curve) as function of shear s and that of ballooning mode α_{BAL} (dashed curve) in (A). The solid curve in (A) is the $\alpha - s$ curve for those pressure and safety-factor profiles shown in (B) and (C).

tion of bootstrap current is driven by the unthermalized fast ions (see Fig. 7), their contribution to the total bootstrap current is much smaller than those by bulk plasma electrons and ions. This implies that the effective β_p to drive neoclassical current is reduced in this region. Consequently, the bootstrap current drops from the linear dependence on β_p. For reference, the ratio of the volume-averaged density of fast ions to the volume-averaged electron density $\bar{n}_f/\bar{n}_e$ for $I_{\rm tot} = 3$ MA is also shown by the dash-dotted curve in Fig. 8.

5.4. *MHD Stability*

At the final stage of ACCOME, MHD stability of the converged plasma current profile is investigated. Typical results are shown in Fig. 9 for calculation parameters $I_{\rm tot} = 3.0$ MA and $n_{e0} = 6 \times 10^{19}$ m^{-3}. Other parameters are as those summarized in Table I. The maximum stable pressure gradient for the Mercier mode $\alpha_{\rm M}$ is shown by the dotted curve as a function of shear s and that of the ballooning mode $\alpha_{\rm BAL}$ by the dashed in (A). The solid curve in (A) is the $\alpha - s$ curve for those pressure and safety-factor profiles shown in (B) and (C). It is evident from Fig. 9 that the converged current profile in the present case is stable against both Mercier and ballooning modes.

6. CONCLUSIONS

A numerical code has been developed for the investigation of beam-driven, ohmic, and bootstrap currents which are consistent with MHD equilibrium. Typical features of the code which is called "ACCOME" are:

(1) The beam-driven current is derived by numerically solving for the eigenfunctions of the bounce-averaged Fokker–Planck equation. Effects of particle trapping, energy diffusion, and bounce motion of fast ions on the beam-driven current are taken into consideration.

(2) The bootstrap current is evaluated for multi-species ions including impurity and fast ions on the basis of the Hirshman–Sigmar moment approach.

(3) An iterative algorithm is employed to obtain non-inductive plasma currents which are consistent with MHD equilibrium.

(4) At the last stage of ACCOME, MHD stabilities for the converged plasma-current profile are investigated analytically.

Applications of ACCOME have been made for parameters appropriate to JT-6OU. Results can be summarized as

(1) To obtain well-converged plasma currents and MHD equilibrium, more than five iterations are necessary.

(2) The effect of particle trapping on the beam-driven current is very important for low $E_{\rm B}/T_e$. The effect exceeds 100% for $E_{\rm B}/T_{e0} < 10$ and is about 30% for $E_{\rm B}/T_{e0} = 40$. The effect of energy diffusion is also important for low $E_{\rm B}/T_{e0,i0}$, but not as important as that of particle trapping for high $E_{\rm B}/T_{e0,i0}$.

(3) NBI power to sustain plasma current without ohmic-power input is estimated. A substantial fraction of NBI power can be saved by the effect of unthermalized fast ions on the bootstrap current.

(4) The bootstrap current is approximately proportional to β_p. The proportionality is broken in both high and low β regions due to the nonlinear effect of bootstrap current on q and the reduction of effective β_p by unthermalized fast ions, respectively.

ACKNOWLEDGMENTS

The authors acknowledge valuable discussions with Drs. S. Yamamoto, N. Fujisawa, M. Matsuoka, T. Tsunematsu, S. Tokuda, and M. Kikuchi. We express our appreciation to Drs. K. Tomabechi, D. E. Baldwin, M. Porklab, D. Overskei, and E. Oktay for their support to our collaboration. Continuous encouragement of Drs. Y. Shimomura, S. Tamura, and M. Yoshikawa is gratefully acknowledged.

REFERENCES

1. R. J. Hauryluk *et al.*, in *Proceedings of the Eleventh International Conference on Plasma Physics and Controlled Nuclear Fusion Research, Kyoto* (IAEA, Vienna, 1987), Vol. 1, p. 51.
2. T. C. Simonen, M. Matsuoka, D. K. Bhadra, *et al.*, *Phys. Rev. Lett.* **61**, 1720 (1988).
3. C. D. Challis, J. G. Cordey, H. Hamnen, *et al.*, *Nucl. Fusion* **29**, 563 (1988).
4. J. E. Stevens, R. E. Bell, S. Bernabei, *et al.*, *Nucl. Fusion* **28**, 217 (1988).
5. K. Ushigusa, T. Imai, Y. Ikeda, *et al.*, *Nucl. Fusion* **29**, 1052 (1989).
6. M. Zarnstorff, M. G. Bell, M. Bitterev, *et al.*, *Phys. Rev. Lett.* **60**, 1306 (1988).
7. D. R. Mikkelsen and C. E. Singer, *Nucl. Technol./Fusion* **4**, 237 (1983).
8. K. Okano, *Plasma Phys. Controlled Fusion* **29**, 1115 (1987).
9. K. Tani, M. Suzuki, S. Yamamoto, and M. Azumi, JAERI-M 88-042, 1988 (unpublished).
10. J. D. Gaffey, *J. Plasma Phys.* **16**, 149 (1979).
11. J. G. Cordey, *Nucl. Fusion* **16**, 499 (1976).
12. J. G. Janev, C. D. Boley, and D. E. Post, *Nucl. Fusion* **29**, 2125 (1989).
13. S. P. Hirshman and D. J. Sigmar, *Nucl. Fusion* **21**, 2079 (1981).
14. Y. B. Kim, J. D. Callen, and H. Hamnen, JET Report R(88)02, 1988 (unpublished).
15. F. L. Hinton and R. D. Hazeltine, *Rev. Mod. Phys.* **48**, 239 (1976).
16. S. P. Hirshman, R. J. Hauryluk, and B. Birge, *Nucl. Fusion* **17**, 611 (1977).
17. M. Azumi and G. Kurita, in *Proceedings, Fourth Symposium on the Computing Methods in Applied Sciences and Engineering, Paris, 1979*, p. 335.